Electronic Properties of $Fe_{3-x}Co_xO_4$ (x = 0.25 and 0.375) Synthesized from Natural Iron Sand: Evaluation of Band Gap and Urbach Tail

Kormil Saputra, Rahmatun Inayah, Ika Umratul Asni Aminy*, Teguh Ardianto, Dian W. Kurniawidi
[1] *Physics Study Program, Faculty of Mathematics and Natural Sciences, University of Mataram, Indonesia*
**email: ikaumratulasni@staff.unram.ac.id*

Abstrak – *Nanopartikel $Fe_{3-x}Co_xO_4$ (x = 0,25 dan 0,375) berhasil disintesis menggunakan pasir besi alami sebagai bahan dasar melalui metode kopresipitasi dengan penambahan $CoCl_2{\cdot}6H_2O$ sebagai sumber kobalt. Karakterisasi optik dilakukan menggunakan spektroskopi UV–Vis pada rentang panjang gelombang 200–800 nm untuk menganalisis sifat elektronik material. Hasil pengukuran menunjukkan bahwa peningkatan fraksi kobalt memperkuat serapan di daerah tampak dan menggeser onset serapan ke energi yang lebih rendah, yang menunjukkan penyempitan energi celah pita. Analisis Tauc menunjukkan bahwa energi celah langsung menurun dari 2,222 menjadi 2,352 eV (x = 0,25), sementara energi celah tidak langsung menurun dari 2,204 eV menjadi 2,388 eV. Lebih lanjut, perhitungan energi Urbach menunjukkan peningkatan dari 0,073 eV pada x = 0,25 menjadi 0,074 eV pada x = 0,375, yang mengindikasikan peningkatan ketidakteraturan lokal yang memperlebar ekor pita. Temuan ini konsisten dengan laporan penelitian sebelumnya tentang magnetit terdoping-ko dan $CoFe_2O_4$, dan menegaskan bahwa doping kobalt efektif dalam meningkatkan kapasitas penyerapan cahaya tampak. Dengan demikian, $Fe_{3-x}Co_xO_4$ berbasis pasir besi alami, terutama pada x = 0,375, memiliki potensi aplikasi sebagai bahan aktif dalam fotokatalisis berbasis cahaya tampak dan perangkat optoelektronik energi surya.*

Kata kunci: *Fe_3O_4, Kobalt, Doping, Optik, Energi.*

Abstract – $Fe_{3-x}Co_xO_4$ nanoparticles (x = 0.25 and 0.375) were successfully synthesized using natural iron sand as the base material through a coprecipitation method with the addition of $CoCl_2{\cdot}6H_2O$ as a cobalt source. Optical characterization was carried out using UV–Vis spectroscopy in the wavelength range of 200–800 nm to analyze the electronic properties of the material. The measurement results showed that increasing the cobalt fraction strengthened the absorption in the visible region and shifted the absorption onset to lower energies, indicating a narrowing of the band gap energy. Tauc analysis revealed that the direct gap energy decreased from 2.222 to 2.352 eV (x = 0.25), while the indirect gap energy decreased from 2.204 eV to 2.388 eV. Furthermore, the Urbach energy calculation shows an increase from 0.073 eV at x = 0.25 to 0.074 eV at x = 0.375, indicating an increase in local disorder that broadens the band tail. This finding is consistent with previous research reports on Co-doped magnetite and $CoFe_2O_4$, and confirms that cobalt doping is effective in enhancing the visible light absorption capacity. Thus, $Fe_{3-x}Co_xO_4$ based on natural iron sand, especially at x = 0.375, has potential applications as an active material in visible light-based photocatalysis and solar energy optoelectronic devices.

Key words: Fe_3O_4, Cobalt, Doping, Optics, Energy

INTRODUCTION

The development of materials science in the last two decades has been heavily influenced by the need for sustainable energy, advanced electronic devices, and nanomaterial-based technologies [1]. One of the main focuses of global research is engineering the electronic and optical properties of semiconductor materials and metal oxides, which are used in various fields, from energy conversion and energy storage to optical sensors and catalysts, to biomedical devices. These materials development efforts are aimed at achieving efficient, stable, easily manufactured systems at low cost, while utilizing abundant natural resources [2]. In this context, transition metal oxides play a crucial role due to their thermal stability, crystal structure flexibility, and ability to be modified through cation substitution and particle size engineering at the nanoscale.

Among various transition metal oxides, magnetite (Fe_3O_4) is one of the most extensively studied due to its unique combination of electronic, optical, and magnetic properties [3]. Fe_3O_4 has an inverse spinel structure, where Fe^{3+} ions occupy tetrahedral sites (A), while a mixture of Fe^{2+} and Fe^{3+} ions occupy octahedral sites (B) [4]. This configuration allows for electron hopping between Fe^{2+} and Fe^{3+}, contributing to its relatively high electrical conductivity at room temperature. Furthermore,

Fe_3O_4 is ferrimagnetic with a large saturation magnetization, making it widely used in magnet-based devices, pigments, catalysts, electrodes, and biomedical applications such as MRI contrast agents and drug delivery.

However, in terms of optical properties, Fe_3O_4 faces challenges. Fe_3O_4 band gap energy is relatively large for visible-light applications, while its optical absorption is limited to specific wavelengths [5]. This relatively wide band gap limits Fe_3O_4 ability to absorb photon energy in the visible spectrum, thus reducing its effectiveness in visible-light-based photocatalysis applications and solar energy optoelectronic devices. In many reports, Fe_3O_4 exhibits semiconducting properties with an optical band gap in the range of 2.2–2.6 eV, which is still less than optimal for full sunlight absorption. Therefore, material engineering strategies are needed to enable Fe_3O_4 to absorb more visible light with higher efficiency. One strategy that has proven effective for modifying the electronic and optical properties of Fe_3O_4 is through doping with transition metal cations [6]. This doping aims to alter the distribution of cations in the spinel lattice, introducing additional energy levels within the band gap, and affecting the density of states (DOS) near the valence and conduction band edges. Previous research has shown that substitution of metal cations such as Ni^{2+}, Mn^{2+}, Zn^{2+}, and especially Co^{2+} can lower the band gap, increase absorption in the visible region, and affect the magnetic and electrical properties of the material [7-9].

Cobalt (Co^{2+}) occupies a crucial position among other transition cations due to its ionic preference for occupying the octahedral (B) site in the spinel structure [10]. The presence of Co^{2+} ions at this site allows direct interaction with Fe^{2+}/Fe^{3+}, which is involved in the electron hopping mechanism. This implies a change in the crystal field (Δoct), strengthening the hybridization of the 3d(Co)–3d(Fe)–2p(O) orbitals, and increasing the density of states near the band edge [9]. Consequently, electronic transitions can occur at lower photon energies, resulting in band gap narrowing and increased absorption in the visible region. Several studies have reported that cobalt doping not only narrows the band gap but also extends the optical response into the near-infrared spectrum, which is highly relevant for photocatalytic applications.

In addition to the band gap, another aspect that needs to be considered in assessing the optical quality of a material is the Urbach energy (E_U). The Urbach energy measures the width of the exponential tail states at the band edge that arise from defects, dislocations, strains, or local potential fluctuations within the crystal. A larger E_U value indicates a higher degree of disorder, while a smaller value indicates better structural order [11]. Thus, Urbach energy measurements can complement band gap analysis to provide a more comprehensive understanding of a material's electronic properties. In the Fe_3O_4 system, Co doping has the potential to not only narrow the band gap, but also increase local disorder, thereby expanding the band tail and influencing the optical transition mechanism.

Several studies support the significant effect of Co doping on the optical properties of ferrite. Zheng et al. [12] reported that cobalt substitution in magnetite increases absorbance in the visible region, accompanied by a decrease in the band gap, although the absolute value of the band gap is strongly influenced by crystallite size and lattice strain. Anantharamaiah and Joy [13] found that $CoFe_2O_4$ nanoparticles have a direct band gap in the range of 1.8–2.1 eV, lower than that of pure magnetite, which is generally >2.2 eV, indicating that Co can narrow the band gap. Todou Assaouka et al. [14] confirmed that the cation distribution and lattice strain due to cobalt doping affect not only the band gap but also the Urbach energy, meaning this doping can alter both the structural regularity and optical properties of the material.

Other studies also support the significant influence of cobalt. Zheng et al. [12] showed that Co-doped ferrite tends to have larger tail states, as reflected by the increased Urbach energy value, due to the increase in local defects in the lattice. Attou et al. [15] reported that Co-doped magnetite synthesized by the coprecipitation method exhibited more stable optical properties compared to doping with other metals, because Co^{2+} more easily fits into the spinel structure. These facts strengthen the rationale for using cobalt as the main dopant for modifying the optical properties of Fe_3O_4. In terms of raw material availability, the use of natural iron sand as a source of Fe^{2+}/Fe^{3+} ions provides significant added value. Iron sand is a very abundant mineral resource in coastal areas of Indonesia, including Loang Balok in West

Nusa Tenggara [16]. So far, iron sand has been mostly used as a raw material for the steel industry, even though its iron oxide content has great potential as a precursor for high-value functional materials such as metal oxide nanoparticles.

The use of natural iron sand as a raw material not only supports the development of locally resource-based nanotechnology but also aligns with the principles of sustainability, increasing the added value of national minerals, and self-sufficiency in raw materials for materials research.

In this context, x = 0.25 and 0.375 were specifically selected to represent low-to-moderate substitution levels that are still structurally safe for the spinel lattice while producing measurable changes in the electronic and optical behavior. Literature on Co-doped magnetite and related spinel systems shows that moderate Co contents are often sufficient to induce clear modifications in magnetic, transport, and band-gap-related properties without destabilizing the host structure or promoting secondary phases [17], [18]. Doping levels below x = 0.25 tend to yield optical and magnetic responses that are very close to those of undoped Fe_3O_4, making systematic trends difficult to distinguish from experimental uncertainty and background effects [19]. Conversely, higher Co contents beyond x = 0.4–0.5 are more prone to inducing significant lattice strain, cation redistribution, and the formation of Co-rich impurity phases—especially under wet-chemical synthesis routes and when natural precursors such as iron sand are used—which complicates phase purity, data interpretation, and the establishment of clear structure–property correlations [17].

Therefore, choosing x = 0.25 and 0.375 provides a rational compromise: the Co content is sufficiently high to reveal clear doping effects on the optical properties, yet still low enough to maintain a predominantly single-phase spinel structure and reliable trends that can be directly attributed to controlled cobalt substitution [17-19]. This study aims to synthesize $Fe_{3-x}Co_xO_4$ nanoparticles based on natural iron sand using a coprecipitation method and analyze their electronic properties through UV–Vis optical characterization, specifically determining the direct and indirect energy gaps using the Tauc method and the Urbach energy as an indicator of structural disorder.

METHOD

Synthesis of $Fe_{3-x}Co_xO_4$ Nanoparticles

The $Fe_{3-x}Co_xO_4$ nanoparticle samples were synthesized using natural iron sand obtained from Loang Balok Beach as the Fe^{2+}/ Fe^{3+} ion source, and $CoCl_2 \cdot 6H_2O$ as the Co^{2+} ion precursor. Based on the chemical formula $Fe_{3-x}Co_xO_4$, two compositions were prepared, namely x = 0.25 and x = 0.375, corresponding to molar ratios of Co:Fe = 0.25:2.75 and 0.375:2.625, respectively. To extract Fe ions, 20 g of iron sand was dissolved in 58 mL of 38% HCl, producing a filtrate containing $FeCl_2.FeCl_3$ after filtration. The concentration of total Fe ions obtained from this process was approximately 0.106 mol. The required amounts of $CoCl_2 \cdot 6H_2O$ were calculated according to the target doping level: for x = 0.25, approximately 2.53 g (0.0106 mol Co^{2+}) was added to the Fe solution; for x = 0.375, approximately 3.79 g (0.0159 mol Co^{2+}) was added. These quantities yielded Co:Fe molar ratios of 0.25:2.75 and 0.375:2.625, in agreement with the nominal compositions $Fe_{2.75}Co_{0.25}O_4$ and $Fe_{2.625}Co_{0.375}O_4$.

Precipitation was carried out by gradually adding 25 mL of 25% NH_4OH under continuous stirring at room temperature until black $Fe_{3-x}Co_xO_4$ precipitates were formed. The precipitates were washed repeatedly with distilled water until neutral pH (7) was achieved, dried at 100ºC for 1 h, and subsequently ground into fine powders.

Optical Band Gap and Urbach Energy Analysis

Optical properties of the $Fe_{3-x}Co_xO_4$ nanoparticles were characterized using a UV–Vis spectrophotometer (LW Scientific V-200-RS, USA) within the wavelength range of 200–800 nm. The optical band gap was determined using the Tauc method [20], which relates the absorption coefficient (α) and photon energy ($h\nu$) through the equation $(\alpha h\nu)^n = A(h\nu - Eg)$, where A is a material-dependent constant and E_g is the optical band gap energy. The exponent n describes the nature of the electronic transition, with $n = 1/2$ representing direct allowed transitions and $n = 2$ corresponding to indirect allowed transitions.

The value of E_g was obtained by extrapolating the linear portion of the $(\alpha h\nu)^n$ versus $h\nu$ plot to the photon energy axis. The Kubelka–Munk method is used as an alternative to the Tauc approach for determining the optical band gap of opaque solids or powder samples. In this method, the diffuse reflectance (R) is converted into the Kubelka–Munk function, F(R), defined as $F(R) = (1 - R)^2/(2R)$ [14]. The quantity F(R) is then treated as an analog of the absorption coefficient (α) in the Tauc relation, so that the band gap can be estimated from the plot of $[F(R) \cdot h\nu]^n$ versus $h\nu$ using the expression $[F(R) \cdot h\nu]^n = A(h\nu - E_g)$.

In addition, the degree of structural disorder was evaluated through the E_U, which characterizes the exponential tail of localized states in the band gap. The absorption coefficient in this region follows the relation $\alpha = \alpha_0 \, exp(\frac{h\nu}{E_U})$, which can be expressed in linear form as $ln(\alpha) = ln(\alpha_0) + \frac{h\nu}{E_U}$. The Urbach energy was obtained from the inverse slope of the linear region in the $ln(\alpha)$ versus $h\nu$ plot [11]. Larger E_U values indicate a broader band tail and a higher degree of lattice disorder, often associated with defects, dislocations, or microstructural irregularities in the crystal.

RESULT AND DISCUSSION

Tests were conducted using a UV–Vis spectrophotometer to obtain transmittance and absorbance curves of $Fe_{3-x}Co_xO_4$ nanoparticles in the wavelength range of 200–800 nm (see Figure 1). The UV–Vis spectrum in Figure 1 shows that increasing the cobalt concentration in $Fe_{3-x}Co_xO_4$ significantly affects the optical absorption characteristics of the material. At a composition of x = 0.25 (Figure 1a), the absorbance curve still shows a relatively lower intensity, while at x = 0.375 (Figure 1b) there is a significant increase in absorbance in the visible region (500–800 nm).

This shift indicates that cobalt doping plays a role in strengthening the optical interaction with visible radiation, making the material more responsive to light with longer wavelengths (redshift). This phenomenon can be explained by the contribution of the 3d (Co^{2+}) orbitals that interact with the 3d(Fe) and 2p(O) bands, thereby increasing the probability of optical transitions in the low-energy region. These results are consistent with reports from several previous studies. Sheng et al. [21] showed that Co^{2+} substitution in Fe-based spinel structures enhances optical absorption in the visible region due to the formation of additional electronic levels around the valence and conduction band edges.

A study by Todou Assaouka et al. [14] on co-doped magnetite also reported an increase in absorbance in the visible region with increasing cobalt fraction, attributed to an increase in the density of states around the Fermi level. Similarly, G. Leonel et al. [22] reported that doping transition cations in magnetite can induce an optical shift toward longer wavelengths, thereby expanding the material's ability to absorb low-energy photons. From a mechanistic perspective, these results are also in line with the findings of Jain [6] who explained that cobalt ions more stably occupy octahedral sites in the spinel structure, thus causing local distortions in the lattice and implicating modifications in the optical properties. This distortion not only increases the absorption intensity but also broadens the absorbable spectrum range. Calculations were then performed to clarify the energy gap values of each sample. The calculations were performed using both the Direct and Indirect methods, the results of which can be seen in Figure 2.

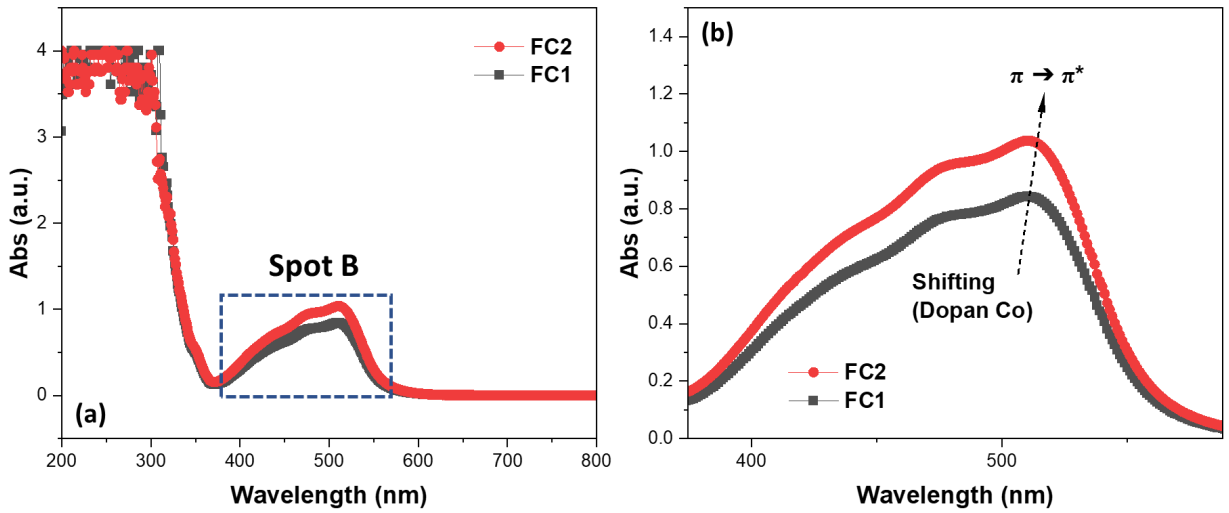

Figure 1. Graph of Absorbance Value of Cobalt-doped Magnetite

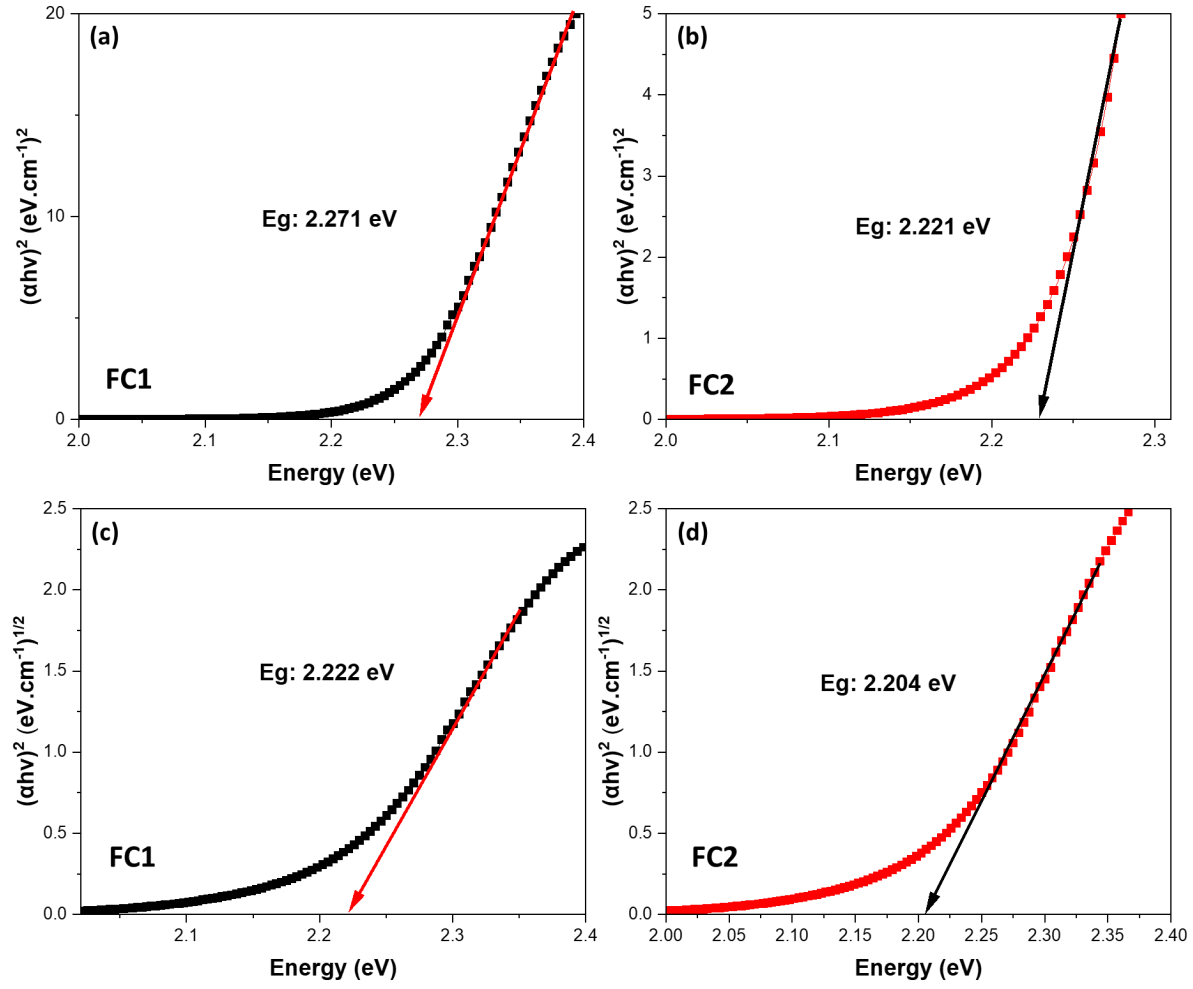

Figure 2. Results of (a to b) Direct Energy Gap; and (c to d) Indirect Energy Gap Calculation for $Fe_{3-x}Co_xO_4$ Samples using the Tauc Plot Method

The UV–Vis spectrum analyzed using the Tauc method shows that the direct energy gap in $Fe_{3-x}Co_xO_4$ changes with increasing cobalt fraction. At x = 0.25 (Figure 2a and Figure 2c), the Tauc curve shows a higher linear region compared to x = 0.375, while at x = 0.375 (Figure 2b and Figure 2d) there is a shift towards lower energy (red-shift) accompanied

by an increase in absorption intensity in the visible region. The direct energy gap value obtained is 2.271 eV, greater than that of x = 0.375, which is 2.221 eV. For indirect result energy gap value obtained is 2.222 eV and 2.204 eV. This phenomenon confirms that Co^{2+} doping introduces additional electronic levels that interact with the 3d(Fe) and 2p(O) orbitals, thereby increasing the chance of direct optical transitions at lower energies.

This finding is in line with the report of Sheng et al. [21] which showed that cobalt substitution in magnetite results in an increase in the density of states near the band edge, which triggers a narrowing of the band gap. Another study by Anantharamaiah and Joy [13] on $CoFe_2O_4$ also reported Egdir values in the range of 1.8–2.1 eV, smaller than those of pure nanocrystalline magnetite, which are typically above 2.2 eV. Similar results were found by Mai et al. [23] who showed a shift in absorption towards longer wavelengths when transition ions such as Co^{2+} were introduced into the spinel structure. This was then followed by calculations using the indirect energy gap method, the results of which can be seen in Figure 3.

Figure 3 shows that increasing the cobalt fraction from x = 0.25 to x = 0.375 consistently strengthens the absorption in the visible region and shifts the absorption onset to lower energies. The indirect energy gap value is 2.315 eV to 2.352 eV for x = 0.25. While at x = 0.375 the value is 2.355 eV to 2.388 eV.

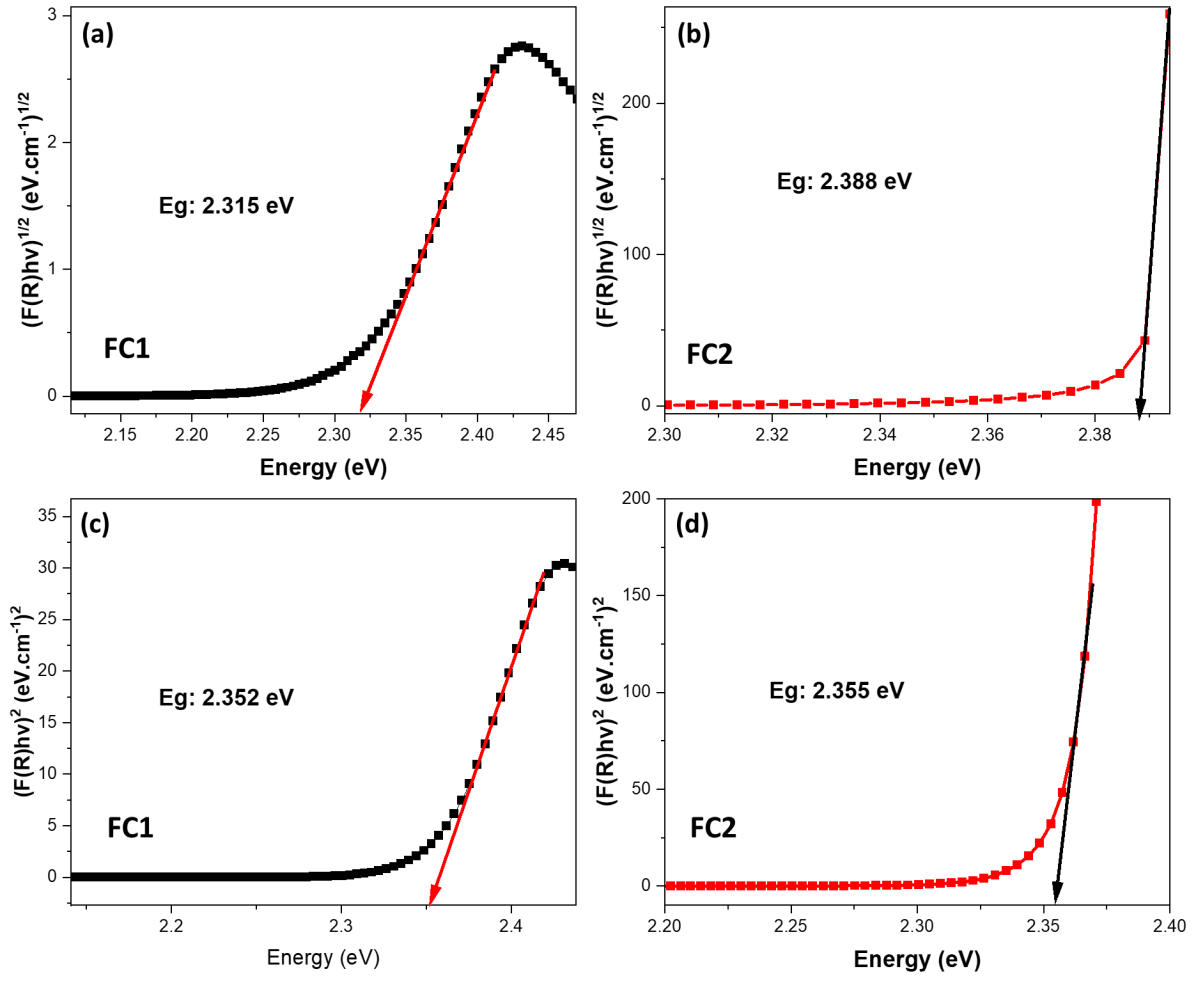

Figure 3. Results of (a) Direct Energy Gap; and (b) Indirect Energy Gap Calculation for $Fe_{3-x}Co_xO_4$ Samples using the Kubelka-Munk Method

In the Kubelka-Munk, both compositions display a clear linear segment, but the sample x = 0.375 (Figure 3c and Figure 3d) shows a cutoff point at a smaller energy and a slightly different slope compared to x = 0.25 (Figure 3a and Figure 3c). Physically, this phenomenon can be interpreted as a consequence of the introduction of Co^{2+} mainly at the octahedral (B) sites in the magnetite inverse spinel, which increases the density of states (DOS) near the

band edge through 3d(Co)–3d(Fe)–2p(O) hybridization. Consequently, the probability of a direct transition without phonon assistance increases at lower photon energies, reflected in a redshift and higher absorption intensity at x = 0.375. This trend is consistent with reports on Co-doped magnetite and nanocrystalline $CoFe_2O_4$, where increasing Co content increases the involvement of 3d(Co) orbitals around the band edge and enhances the visible absorption.

While the absolute values of the reported band gaps vary across studies due to differences in crystallite size, lattice strain, and synthesis methods, the direction of the shift is relatively consistent [24]. In the indirect Tauc plot $(\alpha h\nu)^{1/2}$ vs $h\nu$, both compositions again exhibit a linear region sufficient for extrapolation. Interestingly, the obtained indirect values are very close to the direct values for each composition, with the same compositional trend, namely x = 0.375 still showing an onset at a lower energy compared to x = 0.25.

This closeness indicates that in natural iron sand-based $Fe_{3-x}Co_xO_4$, the absorption mechanism at the optical edge is not monopolized by a single pathway. At the nanoscale, the presence of defects, microstains, and polaronic hopping of Fe^{2+}/Fe^{3+} allows indirect (phonon-assisted) transitions to be active around the absorption edge, allowing the direct and indirect estimates to converge.

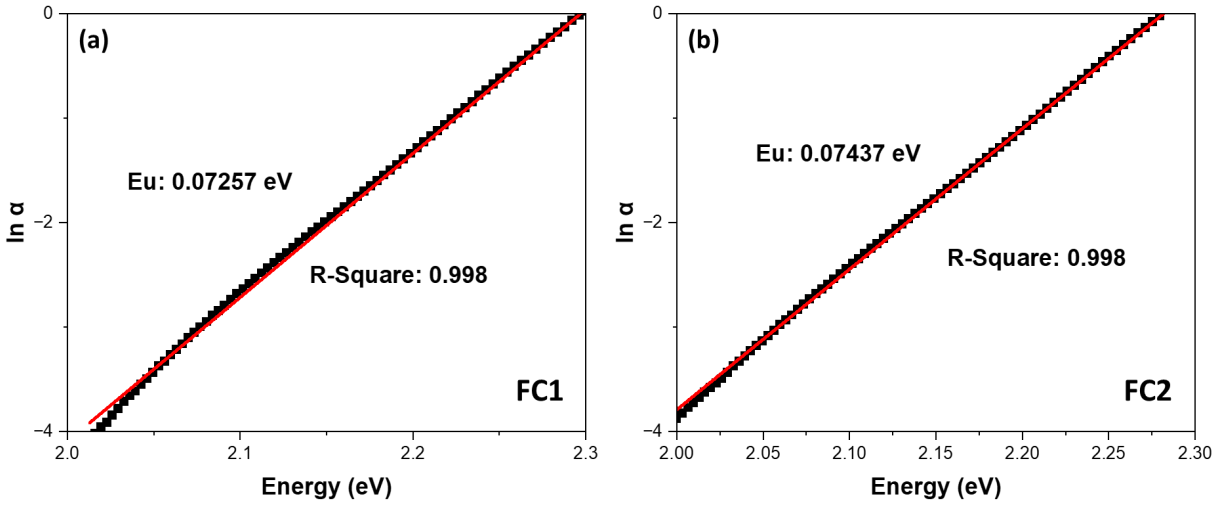

Figure 4. Calculation Urbach Tail of Cobalt Doped Magnetite Nanoparticles

This pattern has also been reported for various spineled ferrites containing Co, where the phonon contribution to momentum conservation becomes significant as the crystallite size decreases or when cation substitution introduces local distortions [12]. Thus, this system exhibits a mixed optical transition: direct remains dominant, but indirect is simultaneously present, so that the absorption onset is relatively stable across different models.

In addition to the onset shift, the spectrum at x = 0.375 exhibits a more pronounced shoulder or ramp in the visible region compared to x = 0.25. This characteristic is commonly associated with band-to-band overlap or mild band tailing due to local disorder, which is again consistent with the role of Co^{2+} as a modifier of the Fe octahedral environment and a 3d-level degeneracy breaker. The literature on Co-based ferrites also indicates that an increase in the visible absorption coefficient is often accompanied by a change in the slope of the Tauc plot, reflecting matrix-element transition modifications and changes in the DOS near the band edges [12], [21]. Given that the starting material used is natural iron sand, microstructural variables such as particle size distribution and minor impurities (common in natural precursors) likely contribute to widening the linear Tauc range, although they do not alter the direction of the main trend between compositions. After calculating the energy gap, the data were backtransformed to obtain the Urbach tail values shown in Figure 4. The Urbach tail (Figure 4) is evaluated from the linear plot of $ln(\alpha)\ vs.\ h\nu$ in the sub-gap region. The slope of the linear segment m is directly related to the Urbach energy through the

relationship $m = \frac{1}{E_U}$; thus, a steeper line larger E_U, indicating a wider band-tail and higher disorder near the band edge.

The Urbach energy (Figure 4) is evaluated from the linear plot of $ln(\alpha)\ vs.\ h\nu$ in the sub-gap region. The slope of the linear segment m is directly related to the Urbach energy through the relationship $m = \frac{1}{E_U}$; thus, a steeper line larger E_U, indicating a wider band-tail and higher disorder near the band edge. Figure 3 shows that $Fe_{3-x}Co_xO_4$ (x = 0.25 and 0.375) exhibits good linearity with Eu values of 0.07257 eV for x=0.25 and 0.7437 eV for x=0.375. The exponential region confirms the presence of tail states due to defects, microstains, and local potential fluctuations—phenomena common to nanocrystalline spinel ferrite. Comparatively, the difference in linear slope between x = 0.25 and x = 0.375 indicates a moderate change in E_U with increasing cobalt. The physical interpretation relates to the substitution of Co^{2+} preferentially occupying octahedral (B) sites in the inverse spinel of magnetite, modifying the Δoct crystal field, affecting the distribution of Fe^{2+}/Fe^{3+} cations, and adding defect centers that widen the band tail. Consequently, the density of localized states near the band edge increases, thus strengthening the sub-gap absorption [25]. This relationship between E_U and the degree of crystalline disorder has been widely reported in ferrites: E_U increases with increasing disorder (strain, defects, impurities). Illustration of Co doping in the Fe_3O_4 structure can be seen in Figure 5.

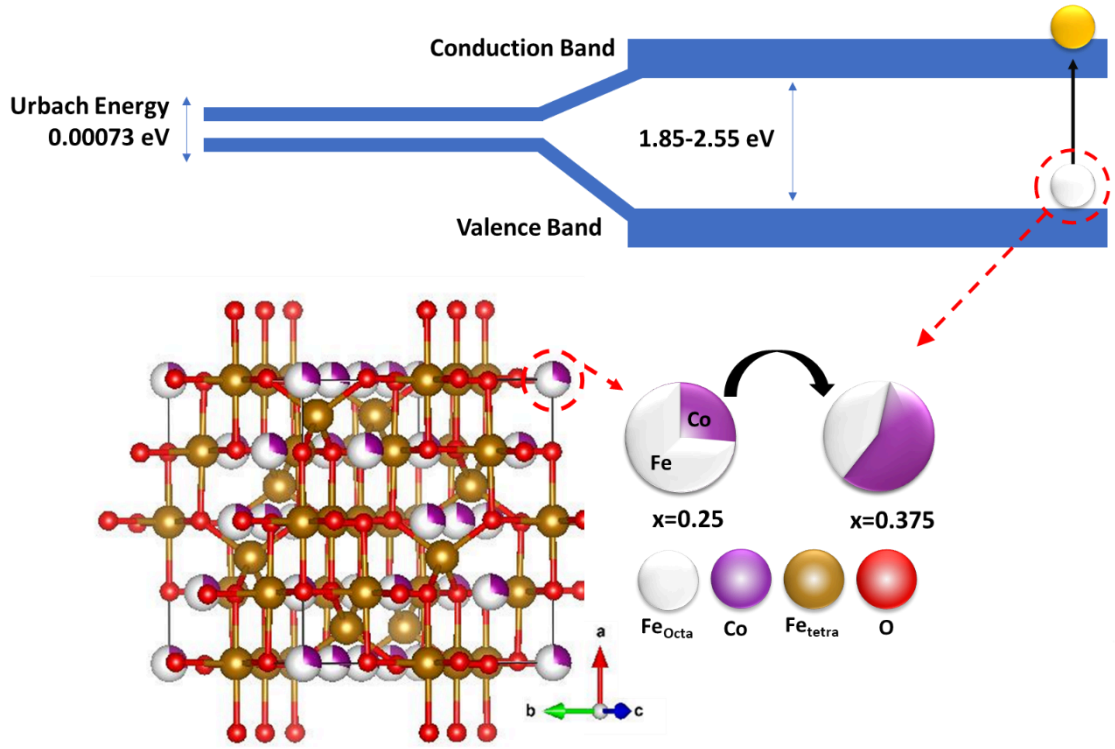

Figure 5. Illustration of Co doping in the Fe_3O_4 Structure

Figure 5 schematically illustrates the incorporation of Co^{2+} ions into the Fe_3O_4 spinel lattice, where partial substitution occurs at the Fe sites within both tetrahedral (A) and octahedral (B) positions. In the ideal Fe_3O_4 structure, Fe^{3+} ions occupy the A-sites while a mixed distribution of Fe^{2+} and Fe^{3+} resides in the B-sites. Upon doping, Co^{2+} ions replace a fraction of Fe cations, as visualized by the highlighted atomic sites in the enlarged lattice representation. This cationic substitution subtly alters the electronic configuration and local bonding environment without disrupting the overall spinel framework, which remains structurally preserved as indicated by the consistent lattice arrangement. The Co–Fe redistribution modifies the local potential landscape and contributes to changes in electronic states near the band edge, which correlates with the observed shift in optical gap

and Urbach energy. The accompanying elemental markers emphasize the controlled Co incorporation and the coexistence of Fe and Co within specific lattice coordinates, reflecting a compositional tuning rather than a structural breakdown of the parent Fe_3O_4 phase. Next, the energy gap results based on Tauc plots and Kubelka-Munk, as well as Urbach energy based on relevant previous research, are compared. The results can be seen in Table 1.

Table 1. Energy Gap and Urbach Energy Values compared with various previous studies

No.	Sample	Tauc Eg (eV)	Kubelka-Munk Eg (eV)	Eu (eV)	Ref.
1.	FC1 ($Fe_{2.75}Co_{0.25}O_4$)	2.222-2.271	2.315-2.352	0.07257	This Study
2.	FC2 ($Fe_{2.625}Co_{0.375}O_4$)	2.204-2.221	2.355-2.388	0.07437	This Study
3.	Fe_3O_4@Yttrium Silicate	5.48-5.49	-	-	[26]
4.	Fe_3O_4/Au	2.77	-	-	[27]
5.	Fe_3O_4	1.4-3.8	-	-	[28]
6.	Un-doped Fe_3O_4	-	2.98	0.666	[29]
7.	Mn-doped Fe_3O_4	-	2.93	0.425	[29]
8.	Zn-doped Fe_3O_4	-	3.01	0.913	[29]
9.	MnS/Fe_3O_4	-	2.85	0.668	[29]
10.	ZnS/Fe_3O_4	-	2.95	0.5368	[29]
11.	$Cu_xFe_{3-x}O_4$ (x=0.05 and 0.1)	1.76-1.83	-	-	[30]
12.	Fe_3O_4@Zn (1-10%)	2.24-2.35	-	-	[31]

The evolution of the E_U in cobalt-containing spinel ferrites is not universal and depends on synthesis conditions, cation distribution within the spinel lattice, and the overall degree of electronic disorder [32], [33]. In $Fe_{3-x}Co_xO_4$ derived from natural iron sand, two features emerge from Table 1. An increase in cobalt content from FC1 to FC2 is accompanied by a modest red shift in the Tauc band gap from 2.222–2.271 eV to 2.204–2.221 eV. Over the same composition interval, E_U changes only slightly from 0.0726 eV to 0.0744 eV, which indicates a minor increase in the density of localized states near the band edge.

When placed against prior reports compiled in Table 1, the present Tauc gaps around 2.20–2.27 eV occupy the mid-visible range that is often reported for modified Fe_3O_4. They are comparable to Fe_3O_4@Zn with values between 2.24 and 2.35 eV [31] and remain below Fe_3O_4/Au at 2.77 eV [27]. They are also far below the very large values reported for Fe_3O_4 embedded in yttrium silicate, namely 5.48–5.49 eV [26]. Relative to the broad envelope reported for Fe_3O_4, which spans 1.4–3.8 eV [28], the present results fall near the center of the distribution and overlap the upper end of the values observed in Cu-doped analogues at 1.76–1.83 eV [30], acknowledging that compositional and analytical differences limit strict one-to-one comparison. The Kubelka–Munk estimates for the present samples, namely 2.315–2.352 eV for FC1 and 2.355–2.388 eV for FC2, remain close to the Fe_3O_4@Zn interval in entry 12 and to other reports that place Fe_3O_4 based materials within the visible regime.

The Urbach energies obtained here, approximately 70–74 meV, are markedly smaller than those listed for undoped and modified Fe_3O_4 in Table 1. Undoped Fe_3O_4 has been reported at about 0.666 eV [29], while Mn- and Zn-doped Fe_3O_4 appear near 0.425 eV and 0.913 eV [29]. Heterostructured systems such as MnS/Fe_3O_4 and ZnS/Fe_3O_4 show values near 0.668 eV and 0.537 eV [29]. Against this backdrop, the present E_U values are lower by roughly an order of magnitude and therefore indicate sharper band edges and a reduced density of tail states without the need to invoke specific microstructural mechanisms. Thus, the E_U trend in $Fe_{3-x}Co_xO_4$ synthesized from natural iron sand is naturally influenced by a combination of composition (x), and residual impurities typical of natural precursors. In practice, a larger E_U is advantageous for broadening the visible absorption through tail states, but potentially increases non-radiative recombination pathways due to the density of localized states; conversely, a smaller E_U indicates sharper band edges and better electronic order—more advantageous for optoelectronic devices that demand clean carrier transport.

CONCLUSION

$Fe_{3-x}Co_xO_4$ nanoparticles (x = 0.25 and 0.375) were successfully synthesized from natural iron sand and showed significant changes in their optical properties due to cobalt doping. The UV–Vis spectra showed an increase in absorbance in the visible region and a shift in the absorption onset to lower energies with increasing cobalt fraction. Tauc analysis showed that the direct gap energy decreased from 2.271 eV (x = 0.25) to 2.221 eV (x = 0.375), while the indirect gap energy decreased from 2.222 eV (x = 0.25) to 2.204 eV (x = 0.375). Urbach energy calculations revealed an increase from 0.07257 eV (x = 0.25) to 0.7437 eV (x = 0.375), indicating increased structural disorder and broadening of the band tail. Thus, increasing cobalt content enhances visible light absorption, narrowing the energy gap, but also increases disorder, confirming a trade-off between optical absorption effectiveness and electronic order. Future studies are recommended to combine optical analysis with advanced structural characterization, such as XPS or Raman spectroscopy, to clarify the relationship between cation distribution, lattice disorder, and the resulting optical properties.

ACKNOWLEDGEMENT

This research was supported by Universitas Mataram under Contract Number **2282/UN18.L1/PP/2025 PDP** on behalf of **Kormil Saputra**. The author gratefully acknowledges this support.

REFERENCES

[1] N. Shakeel, M. I. Ahamed, A. Ahmed, Inamuddin, M. M. Rahman, and A. M. Asiri, ‘Functionalized magnetic nanoparticle-reduced graphene oxide nanocomposite for enzymatic biofuel cell applications’, *International Journal of Hydrogen Energy*, vol. 44, no. 52, pp. 28294–28304, Oct. 2019, doi: 10.1016/j.ijhydene.2019.09.037.

[2] S. Bazsefidpar, M. Freitas, C. Pereira, G. Gutiérrez, and ..., ‘Fe3O4@Au Core–Shell Magnetic Nanoparticles for the Rapid Analysis of E. coli O157:H7 in an Electrochemical Immunoassay’, *Biosensors*, no. Query date: 2025-05-14 09:44:32, 2023, [Online]. Available: https://www.mdpi.com/2079-6374/13/5/567

[3] F. A. S. Da Silva and M. F. De Campos, ‘Study of heating curves generated by magnetite nanoparticles aiming application in magnetic hyperthermia’, *Braz. J. Chem. Eng.*, vol. 37, no. 3, pp. 543–553, Sept. 2020, doi: 10.1007/s43153-020-00063-5.

[4] D. Mishra, J. Nanda, S. Parida, K. J. Sankaran, and S. Ghadei, ‘Effect of Y3+ and Co2+ co-doping on the structural, optical, magnetic and dielectric properties of LaFeO3 nanoparticles’, *J Sol-Gel Sci Technol*, vol. 111, no. 2, pp. 381–394, Aug. 2024, doi: 10.1007/s10971-024-06452-3.

[5] S. Chatterjee, A. Das, A. Das, R. Roy, P. Roy, and ..., ‘Synthesis, evaluation, and biocompatibility study of magnetite nano particles in normal cells and cancer cells for health care application’, *Nano-Structures &Nano ...*, no. Query date: 2025-05-14 09:44:32, 2024, [Online]. Available: https://www.sciencedirect.com/science/article/pii/S2352507X24002245

[6] R. Jain, ‘Effect of gadolinium doping on the Structural, magnetic, Electrical, Optical, and elastic properties of magnetite nanoparticles’, *Materials Science and Engineering: B*, vol. 296, p. 116631, Oct. 2023, doi: 10.1016/j.mseb.2023.116631.

[7] M. Bagherzadeh, *Functionalized MNPs in detection stage of analysis/miniaturization devices*. books.rsc.org, 2021. [Online]. Available: https://books.rsc.org/books/edited-volume/922/chapter/717484

[8] F. Beigmoradi and H. Beitollahi, ‘MXene/La3+ Doped ZnO/Hb Nanocomposite Modified Glassy Carbon Electrode as Novel Voltammetric Sensor for Determination of Hydrogen Peroxide’, *Surface Engineering and Applied ...*, no. Query date: 2025-05-14 09:44:32, 2021, doi: 10.3103/S106837552106003X.

[9] A. El-Shahawy, S. A. Moaty, and ..., ‘Prostate Cancer Cellular Uptake of Ternary Titanate Nanotubes/CuFe2O4/Zn-Fe Mixed Metal Oxides Nanocomposite’, *International Journal ...*, no. Query date: 2025-05-14 09:44:32, 2020, doi: 10.2147/IJN.S228279.

[10] M. González-Sánchez, H. Khadhraoui, and ..., 'Non-enzymatic glucose sensor using mesoporous carbon screen-printed electrodes modified with cobalt phthalocyanine by phase inversion', *Microchemical ...*, no. Query date: 2025-05-14 09:44:32, 2024, [Online]. Available: https://www.sciencedirect.com/science/article/pii/S0026265X24004260

[11] S. Benramache, Y. Aoun, S. Lakel, B. Benhaoua, and C. Torchi, 'The calculate of optical gap energy and urbach energy of Ni1−xCoxO thin films', *Sādhanā*, vol. 44, no. 1, p. 26, Jan. 2019, doi: 10.1007/s12046-018-1003-y.

[12] Y. Zheng, R. Gao, Y. Qiu, L. Zheng, Z. Hu, and X. Liu, 'Tuning Co2+ Coordination in Cobalt Layered Double Hydroxide Nanosheets via Fe3+ Doping for Efficient Oxygen Evolution', *Inorg. Chem.*, vol. 60, no. 7, pp. 5252–5263, Apr. 2021, doi: 10.1021/acs.inorgchem.1c00248.

[13] P. N. Anantharamaiah and P. A. Joy, 'Effect of co-substitution of Co2+ and V5+ for Fe3+ on the magnetic properties of CoFe2O4', *Physica B: Condensed Matter*, vol. 554, pp. 107–113, Feb. 2019, doi: 10.1016/j.physb.2018.11.031.

[14] H. Todou Assaouka *et al.*, 'Copper and iron co-doping effects on the structure, optical energy band gap, and catalytic behaviour of Co 3 O 4 nanocrystals towards low-temperature total oxidation of toluene', *Energy Advances*, vol. 2, no. 6, pp. 829–842, 2023, doi: 10.1039/D3YA00082F.

[15] L. Attou, A. Al-Shami, J. Boujemaâ, O. Mounkachi, and H. Ez-Zahraouy, 'Predicting the structural, optoelectronic, dynamical stability and transport properties of Boron-doped CaTiO3: DFT based study', *Phys. Scr.*, vol. 97, no. 11, p. 115808, Oct. 2022, doi: 10.1088/1402-4896/ac95d8.

[16] S. Susilawati, A. Doyan, and S. Hadisaputra, 'Analysis Magnetic Mineral Content of Natural Iron Sand in Beach Island Lombok as Basic Materials of Micro Wave Absorbers', *Jurnal Penelitian Pendidikan IPA*, vol. 8, no. 4, pp. 1755–1758, Oct. 2022, doi: 10.29303/jppipa.v8i4.2274.

[17] N. Millaty Abadiah *et al.*, 'Nanostructure, Band Gap, and Antibacterial Activity of Spinel Fe2MO4/OO Magnetic Fluids', *IOP Conf. Ser.: Earth Environ. Sci.*, vol. 276, no. 1, p. 012064, May 2019, doi: 10.1088/1755-1315/276/1/012064.

[18] A. Taufiq, R. E. Saputro, D. Yuliantika, A. Hidayat, N. Hidayat, and Sunaryono, 'Exploring magnetic properties and antimicrobial activities of Co0.4Fe2.6O4 ferrofluids using olive oil as dispersant agent', *AIP Conf. Proc.*, vol. 2251, no. 1, p. 030002, Aug. 2020, doi: 10.1063/5.0015623.

[19] K. Saputra, I. U. A. Aminy, R. Inayah, T. Ardianto, and D. W. Kurniawidi, 'Optical Property Enhancement in Cobalt Doped Magnetite Nanoparticles Evaluated with UV Vis Tauc and Urbach', *NMJ*, vol. 6, no. 2, pp. 87–93, Oct. 2025, doi: 10.33369/nmj.v6i2.44047.

[20] J. Tauc, 'Optical Properties of Amorphous Semiconductors', in *Amorphous and Liquid Semiconductors*, J. Tauc, Ed., Boston, MA: Springer US, 1974, pp. 159–220. doi: 10.1007/978-1-4615-8705-7_4.

[21] L. Sheng, H. Tan, L. Zhu, K. Liu, A. Meng, and Z. Li, 'In situ anchored ternary hierarchical hybrid nickel@ cobaltous sulfide on poly (3, 4-ethylenedioxythiophene)-reduced graphene oxide for highly efficient non …', *Microchimica Acta*, no. Query date: 2025-05-14 09:44:32, 2024, doi: 10.1007/s00604-024-06317-0.

[22] A. G. Leonel *et al.*, 'Tunable magnetothermal properties of cobalt-doped magnetite–carboxymethylcellulose ferrofluids: smart nanoplatforms for potential magnetic hyperthermia applications in cancer therapy', Feb. 2021, doi: 10.1039/D0NA00820F.

[23] N. T. T. Mai, N. K. Nga, D. T. M. Hue, T. N. Dung, H. D. Chinh, and T. Q. Huy, 'Characterization of Co2+- and Fe3+-Codoped TiO2 Nanomaterials for Photocatalytic Degradation of Organic Pollutants under Visible Light Irradiation', *Adsorption Science & Technology*, vol. 2021, p. 9193052, Jan. 2021, doi: 10.1155/2021/9193052.

[24] A. Ghosh, D. Ganguly, and R. Sundara, 'A new approach to in-situ uniform growth of

Fe3O4 nanoparticles over thermally exfoliated rGO sheet for the non-enzymatic and enzymatic detection of glucose', *Journal of Electroanalytical Chemistry*, vol. 895, p. 115386, Aug. 2021, doi: 10.1016/j.jelechem.2021.115386.

[25] L. T. H. Phong *et al.*, 'Structural, magnetic and hyperthermia properties and their correlation in cobalt-doped magnetite nanoparticles', *RSC Advances*, vol. 12, no. 2, pp. 698–707, 2022, doi: 10.1039/D1RA07407E.

[26] F. Unal, E. Yucel, Z. C. Orsel, M. F. Akyel, and B. Ercan, 'Synthesis, characterization and cytocompatibility of Fe3O4@yttrium silicate: Samarium nanoparticles with tunable magneto-luminescent properties', *Journal of Alloys and Compounds*, vol. 1036, p. 181885, July 2025, doi: 10.1016/j.jallcom.2025.181885.

[27] Á. de J. Ruíz-Baltazar, 'Sonochemical activation-assisted biosynthesis of Au/Fe3O4 nanoparticles and sonocatalytic degradation of methyl orange', *Ultrasonics Sonochemistry*, vol. 73, p. 105521, May 2021, doi: 10.1016/j.ultsonch.2021.105521.

[28] R. Torres, V. E. Diz, and M. G. Lagorio, 'Improved photosynthetic performance induced by Fe3O4 nanoparticles', *Photochem Photobiol Sci*, vol. 21, no. 11, pp. 1931–1946, Nov. 2022, doi: 10.1007/s43630-022-00269-1.

[29] P. Soltanpour, R. Naderali, and K. Mabhouti, 'Comparative study on structural, morphological, and optical properties of MS/Fe3O4 nanocomposites and M-doped Fe3O4 nanopowders (M = Mn, Zn)', *Sci Rep*, vol. 14, no. 1, p. 21287, Sept. 2024, doi: 10.1038/s41598-024-72026-6.

[30] S. Saleem *et al.*, 'A band gap engineering for the modification in electrical properties of Fe3O4 by Cu2+ doping for electronic and optoelectronic devices applications', *J Sol-Gel Sci Technol*, vol. 109, no. 2, pp. 471–482, Feb. 2024, doi: 10.1007/s10971-023-06287-4.

[31] P. Pietrzyk *et al.*, 'Titan Yellow and Congo Red Removal with Superparamagnetic Iron-Oxide-Based Nanoparticles Doped with Zinc', *Magnetochemistry*, vol. 8, no. 8, p. 91, Aug. 2022, doi: 10.3390/magnetochemistry8080091.

[32] L. C. Sonia and S. Phanjoubam, 'Study on structural, optical and magnetic properties of cobalt substituted magnetite nanoparticles for ferrofluid applications', *Materials Today: Proceedings*, vol. 65, pp. 2883–2888, Jan. 2022, doi: 10.1016/j.matpr.2022.06.434.

[33] M. H. Ayob, W. L. Leaw, D. P. Ramadhani, D. Mariyam, and H. Nur, 'Cobalt Oxide Supported on Silica-Coated Magnetite: Synthesis and Performance in the Photodegradation of Methylene Blue', *ChemistrySelect*, vol. 10, no. 23, p. e05252, 2025, doi: 10.1002/slct.202405252.